

Automated Solar Flare Statistics in Soft X-rays over 37 Years of GOES Observations - The Invariance of Self-Organized Criticality during Three Solar Cycles ¹

Markus J. Aschwanden and Samuel L. Freeland

Lockheed Martin Advanced Technology Center, Solar & Astrophysics Laboratory, Org. ADBS, Bldg.252, 3251 Hanover St., Palo Alto, CA 94304, USA; e-mail: aschwanden@lmsal.com

ABSTRACT

We analyzed the soft X-ray light curves from the *Geostationary Operational Environmental Satellites (GOES)* over the last 37 years (1975-2011) and measured with an automated flare detection algorithm over 300,000 solar flare events (amounting to ≈ 5 times higher sensitivity than the NOAA flare catalog). We find a powerlaw slope of $\alpha_F = 1.98 \pm 0.11$ for the (background-subtracted) soft X-ray peak fluxes that is invariant through three solar cycles and agrees with the theoretical prediction $\alpha_F = 2.0$ of the *fractal-diffusive self-organized criticality (FD-SOC)* model. For the soft X-ray flare rise times we find a powerlaw slope of $\alpha_T = 2.02 \pm 0.04$ during solar cycle minima years, which is also consistent with the prediction $\alpha_T = 2.0$ of the FD-SOC model. During solar cycle maxima years, the powerlaw slope is steeper in the range of $\alpha_T \approx 2.0 - 5.0$, which can be modeled by a solar cycle-dependent flare pile-up bias effect. These results corroborate the FD-SOC model, which predicts a powerlaw slope of $\alpha_E = 1.5$ for flare energies and thus rules out significant nanoflare heating. While the FD-SOC model predicts the probability distribution functions of spatio-temporal scaling laws of nonlinear energy dissipation processes, additional physical models are needed to derive the scaling laws between the geometric SOC parameters and the observed emissivity in different wavelength regimes, as we derive here for soft X-ray emission. The FD-SOC model yields also statistical probabilities for solar flare forecasting.

Subject headings: Sun: corona — Sun: X-rays — Sun: flares — methods: statistical

1. INTRODUCTION

There are a number of intriguing questions that have been raised about statistics of solar flares: (1) Why do they show the ubiquitous powerlaws in their occurrence frequency distributions? (2) Do we understand the numerical values of the powerlaw slopes? (3) Do the powerlaw slopes vary with the solar cycle? (4) Is the solar corona heated by nanoflares? (5) Can the flare statistics be explained in terms of the self-organized criticality (SOC) concept? (6) What are the consequences of SOC models on our physical understanding of solar flares? (7) How can we improve statistical solar flare prediction? (8) What are the largest expected solar flares in history and future? In this paper we address these questions by conducting statistics of solar flares using the longest uniform dataset we have available, namely the soft X-ray light curves from the

¹Manuscript version, 2012-May-28

Geostationary Operational Environmental Satellites (GOES), which cover over 37 years during the period of 1974-2012.

The GOES program consists of a series of geostationary satellites (orbiting the Earth at a height of 35,790 km), which overlap in time so that there are always one to three spacecraft present and guarantee an essentially uninterrupted time series of solar soft X-ray fluxes, besides continuous meteorological observations of the Earth. The GOES-1 satellite was launched on October 16, 1974, and GOES-2 and GOES-3 followed in 1977 and 1978. In the meantime the series continued up to GOES-15, launched on March 4, 2010, while the future satellites GOES-R and GOES-S (with soft X-ray imaging capabilities) are in the queue for a launch in 2015 and 2017, respectively. Operational and technical details of GOES satellites can be gleaned from Grubb (1975), Donnelly et al. (1977), Bouwer et al. (1982), Thomas et al. (1985), Kahler and Kreplin (1991), Garcia (1994), Hill (2005), Pizzo et al. (2005), Shing et al. (1999), White et al. (2005), Neupert (2011), the *National Oceanographic and Atmospheric Administration (NOAA)* website <http://www.oso.noaa.gov/goes/>, or the NASA website <http://goespoes.gsfc.nasa.gov/project/index.html>. For our study we are concerned with the soft X-ray light curves, which are recorded in two energy channels, i.e., in the softer energy range of 1-8 Å and in the harder energy range of 0.5-4 Å. Both light curves are available with a cadence of 3 s, and with a cadence of 2 s after 2009 Dec 1.

Solar flare statistics can be generated by detection of sudden impulsive increases of the soft X-ray intensity in light curves. NOAA publishes solar flare catalogs that are issued on a daily basis. Here we develop an automated flare detection algorithm that allows us to analyze the entire 37-year time series in an objective way without human subjectivity. We are interested in the mathematical function of the probability distributions of solar flare parameters. It has been established earlier that the size distribution of soft X-ray peak fluxes of solar flares have a powerlaw-like form, with a powerlaw slope in the range of $\alpha_P \approx 1.6 - 2.1$ (Hudson et al. 1969, Drake et al. 1971, Shimizu 1995, Lee et al. 1995, Feldman et al. 1997, Shimojo and Shibata 1999, Veronig et al. 2002a,b, Yashiro et al. 2006). In this study we will measure this parameter with the largest available statistics, including over 300,000 detected solar flare events, and will study its variation during three solar cycles. Further we will investigate measurement uncertainties of previously analyzed distributions and compare them with the results from this study in order to establish the most accurate value.

The appearance of powerlaw-like size distribution functions has generally been linked to the theory of self-organized criticality (SOC) (or alternatively to turbulence), which predicts scale-free powerlaw distributions (Bak et al. 1987, 1988). A prominent paradigm of the SOC concept is a sandpile that produces a scale-free distribution of avalanche sizes, once it reaches a critical slope and is slowly driven by random input of dropped sand grains. This concept was also applied to the magnetically driven solar corona, which releases intermittent amounts of nonpotential magnetic energies during flares (Lu and Hamilton 1991). Many applications of SOC processes can be found from geophysics to astrophysics, all the way to financial and social systems. The topic of SOC is reviewed in recent reviews, textbooks, and monographs (e.g., Bak 1996; Jensen 1998; Turcotte 1999; Charbonneau et al. 2001; Hergarten 2002; Sornette 2004; Aschwanden 2011a; Crosby 2011; Pruessner 2012). In this study we go beyond the mere establishment of powerlaw indices, but try also to understand the quantitative values of the observed powerlaw slopes and their variation with the solar cycle. We interpret the observations in terms of a recently published theoretical model based on a statistical fractal-diffusive avalanche model in a slowly-driven self-organized criticality system (Aschwanden 2012). The application of this model allows us also to provide a quantitative framework for statistical flare predictions, which includes also probabilities for the most extreme space weather events.

The content of this paper is as follows: Section 2 presents the data analysis and results, in Section 3

we apply the SOC theoretical model, in Section 4 we compare the results with previous observations, and in Section 5 we summarize the conclusions.

2. DATA ANALYSIS

2.1. Dataset

Our basic data input is the 37-year time series of complete years (from 1975 to 2011) of the GOES softer X-ray channel in the 1-8 Å wavelength range. We choose the softer energy channel (1-8 Å = 1.5-12 keV) over the harder energy range (0.5-4 Å = 3-25 keV) because of its higher sensitivity to smaller flares and less data noise. The data are available in the *Solar Software (SSW)* (Freeland and Handy 1998), originally provided by NOAA, and can be read with IDL software (using the procedure *RD_GXD.PRO*). The data are returned with time tick marks $t_i, i = 1, \dots, N$ for the 3-s intervals and flux values $f_i^\lambda, i = 1, \dots, N$ in physical units of (Wm^{-2}), for both wavelength ranges $\lambda = 1 - 8 \text{ \AA}$ and $\lambda = 0.5 - 4 \text{ \AA}$. The logarithmic flux values are also labeled with letters (A, B, C, M, X-class), which denote the order of magnitude of the peak flux on a logarithmic scale ($A = 10^{-8}, B = 10^{-7}, C = 10^{-6}, M = 10^{-5}, X = 10^{-4} Wm^{-2}$), subdivided with an additional digit (e.g., an X2 class flare has a flux of $2 \times 10^{-4} Wm^{-2}$).

Flare catalogs are issued by NOAA, which provide the peak fluxes, start times, peak times, and end times of flare events, but no preflare background is provided in the flare catalogs, which is important for statistical studies of small flares. If no preflare background is subtracted from the peak flux, the peak flux includes not only the flare-associated flux, but also the total soft X-ray flux of all active regions on the entire solar disk and beyond the limb, which is larger than the flare-associated flux for A, B and C-class flares during active phases of the solar cycle (Wagner 1988; Bornmann 1990; Aschwanden 1994; Veronig et al. 2004). Therefore, proper evaluation of the preflare background requires the analysis of the light curves, and cannot be obtained from the official NOAA flare catalog alone. Furthermore, the GOES light curves contain occasional data gaps (due to Earth occultation, calibration procedures, or drop-outs) and nonsolar spikes (of instrumental, terrestrial, or magnetospheric origin), which need to be removed to avoid false flare detections.

2.2. Automated Flare Detection Algorithm

After testing various automated flare detection algorithms at various background soft X-ray flux levels, which range from the A-level during the solar cycle minimum to the C-level during the solar cycle maximum, by optimizing maximum sensitivity of detecting the smallest flares and by minimizing false detections, we arrived at the following algorithm:

1. Rebinning of data: The intrinsic time resolution of $dt = 3 \text{ s}$ is rebinned to time steps of $\Delta t = 12 \text{ s}$ (matching the SDO/AIA cadence used in another study) by the median value during each bin with length $n_{bin} = \Delta t/dt = 12/3 = 4$. Thus, a daily record has $n_{day} = 86,400/3 = 28,800$ datapoints, which is downsampled to a number of $n_{bin} = 86,400/12 = 7200$ bins.
2. Definition of minimum flare duration: We set a minimum flare duration at a 1-minute time interval, i.e., $\Delta t_{min} = 60 \text{ s}$, which corresponds to a number of $\Delta N_{bin} = 60/12 = 5$ bins.

3. Definition of noise level and threshold: From the mean and standard deviation of typical GOES fluxes during quiescent time periods we find a noise level of $f_{noise} \approx 2 \times 10^{-8} W m^{-2}$, and define a corresponding threshold level of $f_{thresh} = f_{noise}$. The noise level of GOES-8, 9, 10 is constant within less than 10% variation (http://rammb.cira.colostate.edu/research/calibration_validation_and_visualization/goes_image_display/noise.asp).
4. Elimination of data gaps: These are identified by time intervals with a constant “floor” flux value that corresponds to the minimum flux of the daily light curve.
5. Spike removal: Single spikes are detected if the ratio of the maximum flux f_{max} to the minimum flux $f_{min} \geq f_{noise}$ is larger than $q_{spikes} = f_{max}/f_{min} > 10$ during a time interval of $\pm \Delta t_{min} = 60$ s.
6. Smoothing of light curve: We smooth the rebinned light curve with a boxcar of $nsm = 21$ time bins, which corresponds to $nsm \approx 4\Delta N_{bin}$ minimum flare durations.
7. Detection of maxima and minima: We detect now all local maxima and minima of the smoothed light curve (consecutively in daily intervals). The flux maximum times t_i represent candidates for flare peak times, and flux minimum times t_{i-1} and t_{i+1} represent potential flare start and end times.
8. Detection of flare event: Flare events are defined when they fulfill the following conditions (see Fig. 1): (i) The flare starts at a flux minimum time $t_s = t_i$, where a preflare background f_{BG} is defined from the median flux in a time interval $[t_s - \Delta t_{min}, t_s]$; (ii) The flare ends at the first subsequent flux minimum time $t_e = t_{i+1+k}$ with $k > 0$ when the flux drops below the level $f_{BG} + f_{thresh}$, but before the start of a next flare (i.e., no overlapping flare time intervals); (iii) The flare peaks at the highest flux value f_p at time t_p during the intervening time interval $t_s < t_p < t_e$. (iv) The background-subtracted peak flux is $F = f_p - f_{BG}$. Obviously, during solar maximum a lot of flares start on the tail of previous larger events, and thus the background flux is higher, which is not the case during solar minimum. The GOES non-flare background flux varies similarly to the sunspot number (Wagner 1988). - In addition we measure also the steepest flux derivative $(df/dt)_{max}$ during the rise time $[t_s, t_p]$, which can be used as a proxy for the hard X-ray peak flux according to the Neupert effect (Dennis and Zarro 1993).

An example of automated flare detection is shown for 2012-Jan-27 in Fig. 2, when an GOES class X1.8 flare occurred. A total of 36 flare events were detected during this day, mostly ranking in the B and C-class level. In this example we see that the flux of most of the small B and C-class flares returns to a background level of $\approx 5 \times 10^{-7} W m^{-2}$. The duration of larger flares (e.g., C5.5, C3.3, X1.8, C3.5) is truncated by the start of subsequent flares. Therefore, we expect that the flare duration is generally underestimated at times of high flare rates. A more correct flare duration could potentially be derived from a flare decay model that extrapolates the beginning of the flare decay phase all the way to the background level.

We found that this flare detection algorithm is sensitive to the smallest flares recognizable by visual inspection, and at the same time to be fairly robust with an estimated false-detection rate of $\lesssim 10^{-2} \dots 10^{-3}$, based on visual flare classification.

2.3. Flare Rate and GOES Duty Cycle

The monthly rate of detected flares is shown in Fig. 3, for all flares, as well as for the subsets of $> C1.0$, $> M1.0$, and $> X1.0$ flares separately. The total number of detected flares larger than a given

magnitude decreases approximately by a factor of 10 for each order of magnitude: from 338,661 events of all flares to 35,221 > C-class flares, 3986 >M-class flares, to 248 >X-class flares, during a time span of 37 years. The detected flare rate is also shown on a logarithmic scale (Fig. 3 bottom), which shows better the proportionality of detected flares in different magnitudes, even across the minima and maxima of the three solar cycles. There are indeed some months during the last extended solar cycle minimum 2008-2009 with no detected flares at all, which corroborates also the robustness of our detection algorithm for false events by noise coincidence. The number of detected flares per year is listed in Table 1, ranging from a minimum of 186 events per year (2008) to a maximum of 18,797 events per year (1979).

Comparing the number of detected flares with the official GOES flare catalog from NOAA (readable with procedure *GET_GEV.PRO* in *SSW/IDL*), we find 39,696 flare events reported by NOAA during the period of 1991-2011 (the annual number of NOAA events is listed in Table 1, 3rd column). Thus our flare detection algorithm detects 9153 events per year in the average, while the NOAA catalog lists 1804 events per year, so our algorithm is about 5 times more sensitive. The NOAA flare detection algorithm is defined as follows: The event starts when 4 consecutive 1-minute X-ray values have met all three of the following conditions: (i) All 4 values are above the B1 threshold; (ii) All 4 values are strictly increasing; (iii) The last value is greater than 1.4 times the value that occurred 3 minutes earlier. The peak time is when the flux value reaches the next local maximum. The event ends when the current flux reading returns to half of the peak value (<http://www.ngdc.noaa.gov/stp/solar/solarflares.html>).

We determined the effective GOES duty cycle from the number of datapoints that we obtained from reading the GOES database with the SSW standard routine and found an average of $94\% \pm 4\%$ during the years 1978-2011, and a lower fraction of $76\% \pm 8\%$ during the first 3 years of the GOES series (see Table 1). The actual duty cycle of GOES may be higher, because our value of the duty cycle is derived from the number of readable files, and thus the missing data may also include file reading problems, besides the originally missing data (due to data loss, telemetry gaps, calibration procedures, Earth occultation, etc.). Anyway, GOES has probably the highest duty cycle from all solar-dedicated space missions, and thus offers the most complete record of solar flares over the last three solar cycles.

2.4. Occurrence Frequency Distributions

The size distribution of many solar flare parameters has been found to be close to a powerlaw function. However, often there is a gradual turnover at the lower end of the powerlaw range near the detection threshold. In addition, there is sometimes an exponential drop-off apparent at the upper end of the powerlaw range. Since the fit of a powerlaw slope can be severely affected by the gradual turnover at the lower end, we fit a powerlaw function with an empirical correction term that characterizes the turnover with a transition to a constant function at the lower end of the distribution function,

$$N(x)dx = N_1(1 + x/x_1)^{-\alpha}dx . \quad (1)$$

At the low end the distribution converges to a constant $N(x \ll x_1) \mapsto N_1$, while the asymptotic limit at the upper end turns into a pure powerlaw function, $N(x \gg x_1) \mapsto N_1(x/x_1)^{-\alpha}$. We call x_1 the “lower bound” or “turnover value” of the powerlaw range.

The powerlaw fits of the size distribution functions of the soft X-ray flux are shown for each year from 1974 to 2012 separately in Fig. 4, yielding powerlaw slopes in the range of $\alpha_F = 1.7 - 2.3$, with a mean and standard deviation of $\alpha_F = 1.98 \pm 0.11$. The individual values and uncertainties are also listed for every

year in Table 1. The annual fits show in most cases a clear turnover at the lower end, which is well fitted by our empirical function (Eq. 1) and renders the value of the powerlaw slope quite stable, independently of which bins near the turnover are included or excluded in the fit. The accuracy of the powerlaw slope is often hampered in earlier studies due to arbitrary definitions of the fitted range.

In Fig. 5 we compare the powerlaw fits for the GOES peak fluxes for different phases of the solar cycles. We select three different regimes: (i) Years near the solar cycle maximum (defined by periods with more than 10,000 flare events detected per year, see Table 1, second column, which includes the periods of 1978-1982 for Cycle 21, 1988-1991 for Cycle 22, 1998-2003 for Cycle 23, and 2011 for Cycle 24), (ii) Years near the solar cycle minimum (defined by periods with less than 3000 flare events detected per year, which includes the periods of 1975-1976, 1985-1986, 1995-1996, and 2007-2009), and (iii) intermediate time intervals during the rise or decay of solar cycles. The powerlaw fits of these three data subsets exhibit a remarkable constant powerlaw slope of $\alpha_F \approx 2.0$ (Fig. 5, top panel), so that the probability distribution functions differ only by a variable scaling factor for the occurrence frequency as a function of time.

In Fig. 5 (middle panel) we show the same statistics for the parameter of the maximum flux-time derivative $(df/dt)_{max}$ during the rise time of the flare light curve, which also exhibits the same behavior as the soft X-ray peak flux, namely a constant powerlaw slope $\alpha_{df/dt} \approx 2.0$, with a variable scaling factor for the occurrence frequency as a function of time. The powerlaw slopes $\alpha_{df/dt}$ are also tabulated for each year in Table 1. If we would apply the Neupert effect, the time derivative (df/dt) of the soft X-ray flux should be a good proxy of the (smoothed) hard X-ray peak flux, which predicts then a powerlaw slope of $\alpha_P^{pred} = \alpha_{df/dt} = 2.0$. In reality, however, hard X-ray peak rates were found to have a powerlaw slope of $\alpha_P = 1.73 \pm 0.07$ (Aschwanden 2011b). This discrepancy results from a combination of two effects: (i) The simplest formulation of the Neupert effect in terms of an integral (Eq. 21) is oversimplified as we will see below (Section 3.2), and (ii) the time derivative measured from the *smoothed* soft X-ray time profile represents an underestimate of the true time derivative of the unsmoothed light curve.

Finally, we plot also the frequency distribution of flare rise times t_{rise} , which is probably a good proxy for the flare duration T of effective energy release, as measured from non-thermal X-rays light curves and expected from the Neupert effect. We plot the size distributions for the same three epochs of the solar cycle, but find a completely different behavior (Fig. 5, bottom panel). The powerlaw slopes are found to be steepest at the solar cycle maximum with an average slope of $\alpha_T \approx 3.2$, while they become flatter with a value of $\alpha_T \approx 2.3$ at the solar minimum. The values for different years vary from $\alpha_T = 1.75$ (for the year 2008 with the most extreme solar minimum), up to $\alpha_T = 5.18$ (for the year 2002, which represented the peak of the last solar Cycle 23), as it can be seen from the list in Table 1.

2.5. Solar Cycle Variability

Apparently, some soft X-ray parameters vary during the solar cycle, while others do not. For an overview of this time-dependent behavior we plotted the various parameters as a function of time (over the last 37 years) in Fig. 6. The most invariant parameters are the powerlaw slope $\alpha_F \approx 2.0$ of the soft X-ray peak flux and the slope $\alpha_{df/df} \approx 2.0$ of the time derivative, having almost identical values. The largest deviation from a constant value is seen for the year 2009, the year with the second-lowest flare rate ($N_{flare} = 528$), and thus represents a statistical fluctuation due to small-number statistics.

The time variation of the (detected) soft X-ray flare rate is shown in the bottom panel of Fig. 6 (hatched with a grey area). Comparing with this solar cycle variation of the flare rate, we see clearly that the other

parameters plotted in Fig. 6 all exhibit a correlated time variation, which applies to the powerlaw slope α_T of the flare rise time T (Fig. 5, 3rd panel), the turnover value P_1 of the peak count rate P (corresponding to the symbol x_1 in Eq. 1) (Fig. 5, 4th panel), the turnover value $(df/dt)_1$ of the time derivative (df/dt) (Fig. 5, 5th panel), and the turnover value T_1 of the rise time T (Fig. 5, 6th panel). In all these parameters, the turnover value seems to fluctuate in synchronization with the flare rate. This implies that the degree of undersampling of weak flares becomes more severe for times with higher flare rates, especially during the solar cycle maxima. This behavior is apparently a feature of our automated flare detection algorithm, which detects a smaller number of flares during periods of high activity, either because the flux contrast for small flares is relatively weaker on top of a light curve of a large flare, compared with the background noise level during quiescent times. In addition, the rule that each flare is separated in time and does not allow for temporal overlap (of rise times), may suppress the recording of smaller flares during the evolution of a larger flare. Actually, we will demonstrate in the following theoretical section that this effect can be simply modeled and predicted as a function of the instantaneous flare rate (Section 3.3).

3. THEORETICAL MODEL

We apply now the statistical fractal-diffusive (FD-SOC) avalanche model of a slowly-driven self-organized criticality (SOC) system, which is derived in general form for all 3 Euclidean dimensions $S = 1, 2, 3$ and tested with cellular automaton simulations in a recent paper (Aschwanden 2012). For our application to soft X-ray data from solar flares here we consider only the 3D case ($S = 3$) and add a simple physical model of the soft X-ray (thermal) radiation mechanism (Section 3.2).

3.1. The Fractal-Diffusive Avalanche SOC Model

The fractal-diffusive SOC model is a universal (physics-free) analytical model that describes the statistical time evolution and occurrence frequency distribution function of SOC processes. It is based on four fundamental assumptions: (1) A SOC avalanche grows spatially like a diffusive process; (2) The spatial volume of the instantaneous energy dissipation rate is fractal; (3) The time-averaged fractal dimension is the mean of the minimum dimension $D_{S,min} \approx 1$ (for a sparse SOC avalanche) and the maximum dimension $D_{S,max} = S$ (given by the Euclidean space); and (4) The occurrence frequency distribution of length scales is reciprocal to the size L of spatial scales, i.e., $N(L) \propto L^{-S}$ in Euclidean space with dimension S . We will discuss these assumptions in more detail in the following.

The first assumption of a diffusive process is based on numerical simulations of cellular automaton models. A SOC avalanche propagates in a cellular automaton model by next-neighbor interactions in a critical state, where energy dissipation propagates only to the next neighbor cells (in a S -dimensional lattice grid) that are above a critical threshold. This mathematical rule that describes the entire dynamics and evolution of a SOC avalanche is very simple for a single time step, but leads to extremely complex spatial patterns after a finite number of time steps. For a visualization of a large number of such complex spatial patterns generated by a simple iterative mathematical redistribution rule see, for instance, the book “A New Kind of Science” by Wolfram (2002). The complexity of these spatial patterns can fortunately be characterized with a single number, the fractal dimension D_S . If one monitors the time evolution of a spatial pattern of a SOC avalanche in a cellular automaton model, one finds that the length scale $x(t)$ evolves with

time approximately with a diffusive scaling (Section 2.1 in Aschwanden 2012),

$$x(t) \propto t^{1/2} , \quad (2)$$

which leads to a scaling law between the avalanche sizes $L = x(t = T)$ and time durations T of SOC avalanches,

$$L \propto T^{1/2} . \quad (3)$$

The second assumption of a fractal pattern of the instantaneous energy rate is also based on tests with cellular automaton simulations (see Fig. 2 in Aschwanden 2012). The fractal dimension is essentially a simplified parameter that describes the “micro-roughness”, “graininess”, or inhomogeneity of critical nodes in a lattice grid in the state of self-organized criticality. Of course, such a single number is a gross oversimplification of a complex system with a large number of degrees of freedom, but the numerical simulations confirm that it reproduces the correct scaling law between the instantaneous energy dissipation volume $V_S(t)$ and the spatial scale $x(t)$ of SOC avalanches,

$$V_S(t) \propto x^{D_S} , \quad (4)$$

which leads also to a statistical scaling law between avalanche volumes V and spatial scales L or durations T (with Eq. 3) of SOC avalanches,

$$V_S \propto L^{D_S} \propto T^{D_S/2} . \quad (5)$$

The third assumption of the mean fractal dimension has also been confirmed by numerical simulations of cellular automaton SOC processes in all three dimensions $S = 1, 2, 3$ (Aschwanden 2012), but it can also be understood by the following plausibility argument. The sparsest SOC avalanche that propagates by next-neighbor interactions is the one that spreads only in one spatial dimension, and thus yields an estimate of the minimum fractal dimension of $D_{S,min} \approx 1$, while the largest SOC avalanche is almost space-filling and has a volume that scales with the Euclidean dimension, $D_{S,max} = S$. Combining these two extreme cases, we can estimate a time-averaged fractal dimension from the arithmetic mean,

$$\langle D_S \rangle \approx \frac{D_{S,min} + D_{S,max}}{2} = \frac{1 + S}{2} , \quad (6)$$

which yields a mean fractal dimension of $\langle D_3 \rangle = (1 + 3)/2 = 2.0$ for the 3D case ($S = 3$).

The last assumption of the size distribution is a probability argument. The system size L_{sys} of a SOC system represents an upper limit of spatial scales L for SOC avalanches, i.e., $L \leq L_{sys}$. For the 3D-case, the volumes V of individual avalanches are also bound by the volume V_{sys} of the system size, i.e., $V = L^3 \leq V_{sys} = L_{sys}^3$. If the entire system is in a critical state, SOC avalanches can be produced everywhere in the system, and the probability $N(L)$ for a fixed avalanche size L with volume V is simply reciprocal to the size, i.e.,

$$N(V) \propto \frac{V}{V_{sys}} \propto V^{-1} , \quad (7)$$

which is equivalent to

$$N(L) \propto \frac{L^3}{L_{sys}^3} \propto L^{-3} . \quad (8)$$

Based on this model we simulate now an example of a time evolution of SOC parameters for the 3D case, as shown in Fig. 7. We start with a mean fractal dimension $\langle D_3 \rangle = 2.0$, and simulate the time

evolution of the fractal dimension $D_3(t)$ by simulating fluctuations with a relatively small amplitude (with a standard deviation of $\sigma_D = 0.15$) by a random generator (Fig. 7 top panel). The time evolution of the instantaneous energy dissipation rate $f(t)$ in classical SOC systems (with a constant mean dissipated energy quantum $\langle \Delta E \rangle$ per unstable lattice node) is then proportional to the instantaneous volume $V_S(t)$, which yields the following function (with Eq. 4),

$$f(t) = \frac{de(t)}{dt} \propto \langle \Delta E \rangle V_S(t) = \langle \Delta E \rangle x(t)^{D_S} = \langle \Delta E \rangle t^{D_S/2} . \quad (9)$$

In the 3D case with $D_S = 2$, we expect than the proportionality $f(t) \propto t^{1.0}$, as shown in Fig. 7 (second panel).

The statistical peak value $p(t)$ of the energy dissipation rate after time t can be estimated from the largest possible avalanches, which have an almost space-filling dimension $D_S \lesssim S$, and thus would be expected to scale as $p(t) \propto t^{S/2} \propto t^{1.5}$ (indicated with a dashed curve in Fig. 7, second panel).

The evolution of the total dissipated energy $e(t)$ after time t is simply the time integral, for which we expect

$$e(t) = \int_0^t \frac{de(\tau)}{d\tau} d\tau \propto \int_0^t \tau^{D_S/2} \propto t^{(1+D_S/2)} , \quad (10)$$

which yields the function $e(t) \propto t^2$ for the 3D case (Fig. 7, third panel). These time evolutions apply to every classical SOC model and can be derived from purely statistical probability arguments, and thus are physics-free. For application to real-world data we have to understand the physical nature of the observables, before we can relate the measured distributions to the statistical SOC theory, which we undertake in the next Section.

3.2. SOC Application to Solar Flare Soft X-ray Data

SOC theory has been applied to different wavelength regimes of solar flare observations, such as to gamma-rays, hard X-rays, soft X-rays, and extreme ultra-violet (EUV). A comprehensive review of such studies is given in Section 7 of Aschwanden (2011a). However, since each wavelength range represents a different physical radiation mechanism, we have to combine now the physics of observables with the (physics-free) SOC statistics.

Soft X-ray emission during solar flares is generally believed to result from thermal free-free and free-bound radiation of plasma that is heated in the chromosphere by precipitation of non-thermal electrons and ions, and which subsequently flows up into coronal flare (or post-flare) loops, a process called “the chromospheric evaporation process” (for a review see, e.g., Aschwanden 2004). Therefore, we can consider the flare-driven chromospheric heating rate as the instantaneous energy dissipation process of a SOC avalanche, as shown in the simulated function $f(t)$ in Fig. 7 (second panel). The heated plasma, while it fills the coronal flare loops, loses energy by thermal conduction and by radiation of soft X-ray and EUV photons, which generally can be characterized by an exponential decay function after an impulsive heating spike. In Fig. 7 (bottom) we mimic such a soft X-ray radiation light curve by convolving the instantaneous energy dissipation rate $f(t)$ (Fig. 7, second panel) with an exponentially decaying radiation function (with an e-folding time constant of τ_{decay}),

$$f_{sxr}(t) = \int_{-\infty}^t f(t') \exp[-(t-t')/\tau_{decay}] dt' , \quad (11)$$

which shows also a time dependence that follows approximately

$$f_{sxr}(t) \propto f(t) \propto t^{1.0}, \quad (12)$$

because the convolution with an exponential function with a constant e-folding time constant acts like a constant multiplier. In the limit of infinitely long decay times ($\tau_{decay} \mapsto \infty$), our convolution function (Eq. 11) turns into a time integral of the heating function $f(t)$, which is also known as Neupert effect (Dennis and Zarro 1993; Dennis et al. 2003), where the heating function is identified with the non-thermal hard X-ray emission and the time integral with the soft X-ray emission. However, such an approximation would predict different values for the powerlaw slopes of hard X-ray and soft X-ray peak fluxes, which was found to contradict the data (Lee et al. 1995). Hence, we consider the formulation of the Neupert effect in terms of a convolution with a finite cooling time (Eq. 11) as a more accurate representation than the time integral formulation (with an infinite cooling time).

We can now calculate the occurrence frequency distributions. The total duration T of energy release corresponds essentially to the rise time t_{rise} of the soft X-ray flux, because the decay phase of a soft X-ray flare light curve is dominated by conductive and radiative loss, rather than by continued heating input. Thus, starting from the size distribution of length scales, $N(L) \propto L^{-S}$ (Eq. 8), we can derive the size distribution of rise times $T = t_{rise}$ by substituting the variable T for L in the distribution $N(L)$, using the diffusive scaling $L(T) \propto T^{1/2}$ (Eq. 3), with the derivative $dL/dT = T^{-1/2}$,

$$N(T)dT = N(L[T]) \left| \frac{dL}{dT} \right| dT \propto T^{-(1+S)/2} dT = T^{-2} dT, \quad (13)$$

yielding $N(T) \propto T^{-2}$ for $S = 3$. Subsequently we can derive the size distribution $N(F)$ of the energy dissipation rate $F = f(t = T)$, using the relationship $F(T) \propto T^{Ds/2}$ (Eq. 9),

$$N(F)dF = N(T[F]) \left| \frac{dT}{dF} \right| dF \propto F^{-[1+(S-1)/Ds]} = F^{-2} dF. \quad (14)$$

Thanks to the proportionality between the functions $f(t)$ and $f_{sxr}(t)$ (Eq. 12), we have also a proportionality between the statistical expectation values $F = f(t = t)$ and $F_{sxr} = f_{sxr}(t)$, and thus a size distribution with an identical powerlaw index,

$$N(F_{sxr})dF_{sxr} \propto F_{sxr}^{-[1+(S-1)/Ds]} = F_{sxr}^{-2} dF_{sxr}. \quad (15)$$

Thus, our theory predicts a powerlaw slope of $\alpha_F = 2.0$ for the soft X-ray fluxes (Eq. 15), and an identical slope of $\alpha_T = 2.0$ for the rise time $t_{rise} = T$ (Eq. 13). As we can see in the observations shown in Fig. 6, the powerlaw slopes of the soft X-ray fluxes has an annually averaged powerlaw slope of $\alpha_F = 1.98 \pm 0.11$, which is moreover invariant over a time span of 37 years, and thus is fully consistent with our theoretical prediction of $\alpha_F = 2.0$. The powerlaw slopes of soft X-ray rise times have a minimum value of $\alpha_T \gtrsim 2.0$ during the solar cycle minima (Fig. 6, third panel), but deviate up to $\alpha_T \lesssim 5.0$ during solar cycle maxima. Apparently there is a solar cycle effect that modifies the theoretically predicted value, which we interpret as a measurement bias in the next Section.

3.3. Solar Cycle Dependence of Flare Pile-Up Bias

Our theory predicts an occurrence frequency distribution of $N(T) \propto T^{-2}$ for flare durations (or rise times in soft X-ray light curves) in the slowly-driven limit where subsequent avalanches do not overlap in

time. Also, our automated flare detection algorithm does not allow for overlapping flare time intervals. However, it is conceivable that the flare rate is so high during the most active times of the solar cycle that multiple flares overlap each other, which violates the slowly-driven condition and leads to an underestimate of the flare durations (because of our rule that a flare has to end before the next flare starts), especially during large and long flares, a bias that leads to a steepening of the powerlaw slope. Indeed we observe powerlaws that are steeper up to a value of $\alpha_T = 5.18 \pm 0.55$ (in the year 2002 near the maximum of the last solar cycle). Thus we try to estimate this effect, which we call “flare pile-up bias”.

The average waiting time between two subsequent flares per year (with a duration of $365.25 \times 86,400$ s = 3.2×10^7 s) is

$$\langle \Delta t_{wait} \rangle = \frac{3.2 \times 10^7 \text{ s}}{N_{flare}}, \quad (16)$$

which varies between $\langle \Delta t_{wait} \rangle = 3.2 \times 10^7 \text{ s} / 18,797 \approx 1700 \text{ s} \approx 28 \text{ min}$ (in the year 1979) to $\langle \Delta t_{wait} \rangle = 3.2 \times 10^7 \text{ s} / 186 \approx 170,000 \text{ s} \approx 2 \text{ days}$ (in the year 2008). The latter year is sufficiently low to fulfill the slowly-driven condition, because the flares are so sparse that they never overlap. However, the former year with an average waiting time of 1.7×10^3 s is significantly shorter than the longest measured flare rise time ($t_{rise} \lesssim 10^{4.5}$ s) and thus underestimates the longer flare durations. We estimate the effect of this flare pile-up bias on the measurement of the powerlaw slope, which is generally defined as,

$$\alpha_T = -\frac{\log(N_2/N_1)}{\log(T_2/T_1)}, \quad (17)$$

with T_1 and T_2 the lower and upper bound of the powerlaw range, and N_1 and N_2 the corresponding number of flares at these boundaries. In the case of flare pile-ups the upper limit T_2 is limited by a time scale that approximately corresponds to the average waiting time $\langle \Delta t_{wait} \rangle$, modifying the observed powerlaw slope α_T^{obs} to

$$\alpha_T^{obs} = -\frac{\log(N_2/N_1)}{\log(\langle \Delta t_{wait} \rangle / T_1)}. \quad (18)$$

for $\langle \Delta t_{wait} \rangle < T_2$. From years with sparse flare rates fulfilling the slowly-driven condition we find $\log(N_2/N_1) \approx 5.2$, $\log(T_2/T_1) \approx 2.6$, yielding $\alpha_T^{obs} \approx 2.0$. Combining Eq. (16) and (18) we obtain a time-dependent powerlaw index that depends on the annual flare rate $N_{flare}(t)$ as,

$$\alpha_T^{obs}(t) = -\frac{\log(N_2/N_1)}{\log(3.2 \times 10^7 / N_{flare}(t) T_1)}, \quad (19)$$

if $N_{flare} \geq 3.2 \times 10^7 / T_2$. We calculate this time-dependent powerlaw index $\alpha_T^{obs}(t)$ for all years (1975-2011) and display the expected curve in Fig. 6 (3rd panel), which closely mimics the powerlaw rate variation $\alpha_T^{obs}(t)$ inferred from the observations. Thus, we conclude that the correct powerlaw slope of $\alpha_T = 2.0$ predicted by SOC theory can be measured during solar cycle minima, while flare pile-up causes a steeper powerlaw slope during solar cycle maxima.

4. DISCUSSION

4.1. Comparison with Previous Statistics

The size distributions of soft X-ray peak fluxes of solar flares have been reported from various spacecraft data, with powerlaw indices in the range of $\alpha_P \approx 1.6 - 2.1$ (Hudson et al. 1969, Drake et al. 1971, Shimizu

1995, Lee et al. 1995, Feldman et al. 1997, Shimojo and Shibata 1999, Veronig et al. 2002a,b, Yashiro et al. 2006). A compilation of these studies is listed in Table 2. Let us quickly review these results, particularly under the aspect of compatibility with our new results.

Probably the first size distribution of soft X-ray fluxes from solar flares was reported for 177 events observed with OSO-3 by Hudson et al. (1969). The cumulative size distribution shows a powerlaw slope of $\beta_P \approx 0.85$ and a gradual turnover at the lower end, which corresponds to $\alpha_P = \beta_P + 1 \approx 1.85$ and is roughly consistent with SOC theory ($\alpha_P = 2$), given the small-number statistics.

A larger statistics of 3140 flare events was gathered with the Explorer spacecraft (Drake et al. 1971), finding a powerlaw slope of $\alpha_P = 1.84 \pm 0.02$ if the fit extended to the third-lowest bin, and a flatter value of $\alpha_P = 1.66 \pm 0.02$ if the fit extended to the second-lowest bin. Clearly, the turnover at low values flattens the powerlaw slope as expected, a systematic error that is not included in the error bars. The same study finds also a powerlaw slope of $\alpha_E = 1.44 \pm 0.01$ for the fluence, and thus is largely consistent with SOC theory ($\alpha_P = 2.0, \alpha_E = 1.5$).

Shimizu (1995) sampled active region brightenings with Yohkoh, which we consider as “miniature flares”. Measuring the peak soft X-ray intensities averaged over 8×8 macropixels, he found a powerlaw slope of $\alpha_P = 1.80$, and $\alpha_P = 1.68$ for 16×16 macropixels, while the powerlaw of energies was found to be $\alpha_E \approx 1.5 - 1.6$, which is largely consistent with SOC theory ($\alpha_P = 2.0, \alpha_E = 1.5$). Another study on Yohkoh active region brightenings reported a less accurate value of $\alpha_P = 1.7 \pm 0.4$ (Shimojo and Shibata 1999), due to the relatively small sample of 92 events.

Lee et al. (1995) reported powerlaw slopes of $\alpha_P = 1.86$ for soft X-ray peak fluxes observed with BCS/SMM, and a slope of $\alpha_P = 1.86$ for a sample of 4356 GOES events. A similar value of $\alpha_P = 1.88 \pm 0.21$ was reported by Feldman et al. (1997), all within about 5% of the theoretically predicted value.

A larger dataset of GOES flares during the years of 1986-2000 was analyzed by Veronig et al. (2002a), yielding a powerlaw index of $\alpha_P = 1.98 \pm 0.08$ after preflare background subtraction, which is perfectly consistent with SOC theory and the values obtained in this study ($\alpha_P = 1.98 \pm 0.11$). In a related study with 49,409 GOES flares, where no preflare background was subtracted, a value of $\alpha_P = 2.11 \pm 0.13$ was found (Veronig et al. 2002b). Since the powerlaw range covered only medium-size to large flares, the background subtraction that is important for small events did not spoil the powerlaw fit. The powerlaw fit of soft X-ray flare durations was found to be $\alpha_T = 2.93 \pm 0.12$. This is not inconsistent with our findings, because this powerlaw index was found to vary in the range of $\alpha_T \approx 2 - 5$ from the minimum to the maximum of the solar cycle, which we interpret as flare pile-up bias.

Very similar values were reported for GOES flares during the period of 1996-2005 (Yashiro et al. 2006), with $\alpha_P = 2.16 \pm 0.03$ for all flares, and $\alpha_P = 1.98 \pm 0.05$ for flares with CMEs. The complementary subset of flares without CMEs have a higher value of $\alpha_P = 2.52 \pm 0.03$, which can be understood as a selection effect that preferentially excludes the larger flares, and thus is expected to produce a steeper powerlaw slope. The flare durations showed powerlaw slopes in the range of $\alpha_T \approx 2.5 - 3.2$ for the same subsets, which can also be understood in terms of the flare pile-up bias.

In summary, all previous measurements are consistent with the theoretically predicted powerlaw slope of $\alpha_P = 2.0$, if we take the uncertainties of small-number statistics and the turnover at the lower bound of the powerlaw range into account. The distribution of flare durations was generally reported to be higher ($\alpha_T \approx 2.5 - 3.2$) than the theoretically predicted value $\alpha_T = 2.0$, but can be satisfactorily understood in terms of the flare pile-up bias effect.

4.2. Coronal Heating by Nanoflares

If a powerlaw distribution of flare energies E is derived, the critical slope of $\alpha_{E,crit} = 2.0$ decides whether the integral of the differential flare energy distribution diverges at the lower or upper end of the powerlaw range (Hudson et al. 1991). Our SOC model, which is increasingly supported by previous observations (Aschwanden 2011b,c) as well as with the new analysis presented here, predicts a powerlaw slope of $\alpha_E = 1.5$ for total time-integrated energies, which is also consistent with observed occurrence frequency distributions in hard X-rays (e.g., $\alpha_E = 1.53 \pm 0.02$; Crosby et al. 1993). Based on this agreement between the theoretical and observational results there is neither a theoretical prediction nor observational evidence for a powerlaw slope α_E steeper than the critical value of $\alpha_{E,crit} = 2$. In addition, the theoretical SOC model predicts a powerlaw slope of $\alpha_P = 2.0$ for peak energy dissipation rates, which requires an energy slope of $\alpha_E = 1.5$ to be consistent with SOC theory. This has also been confirmed in this study, which further corroborates the theoretical SOC model. Based on this argument we conclude that nanoflares have only a negligible contribution to coronal heating.

4.3. Physical Aspects of the SOC Model

What do we learn about the physics of solar flares by applying a statistical SOC model? The classical cellular automaton model mimics the complex spatial and temporal patterns that result in a nonlinear energy dissipation process, without involving a physical mechanism. However, it is thought that a solar flare consists of a fragmented energy release process (Benz 1985), which is manifested in a highly intermittent time structure of decimetric radio emission or nonthermal hard X-ray emission (with time structures down to milliseconds). Numerical MHD simulations can reproduce such a intermittent time evolution in chain reactions of tearing-mode instabilities and magnetic island formation (e.g., Sturrock 1966; LeBoeuf et al. 1982; Tajima et al. 1987; Kliem 1990, 1995; Karpen et al. 1995; Drake et al. 2006a,b), leading to fractal current sheets (Shibata and Tanuma 2001). What the SOC model tells us are the scaling laws between the energy dissipation rate, total dissipated energy, spatial scales, and flare durations, since the power indexes of the correlated parameters are linked to the powerlaw distributions of these parameters. While SOC theory provides the statistical framework of basic spatio-temporal parameters (such as time scales, length scales, and fractal volume scaling), the physics comes into the problem by connecting the observables (i.e., flux intensities at different wavelengths) to the geometric SOC parameters, which involves physical modeling in terms of electron densities, electron temperatures, thermal, and nonthermal energies.

In this study we found that the powerlaw slopes are consistent with the assumption that the emitted soft X-ray flux during a solar flare is proportional to the fractal flare volume (Eq. 9), i.e., $f_{sxr}(t) \propto f(t) \propto V_S(t)$. Given the fact that soft X-ray emission consists of thermal free-free emission, which in the optically-thin limit has a proportionality of the emission measure to the squared density in a volume element cell dV ,

$$f_{sxr} \propto EM_{sxr} \propto \int n_e^2 dV, \quad (20)$$

the emissivity per volume cell is expected to depend on the electron density. Physical modeling is required to quantify the soft X-ray emissivity and emission measure per volume element in a given wavelength range as a function of the volumetric heating rate, conductive, and radiative loss rate (e.g., Metcalf and Fisher 1995; Phillips and Feldman 1995; Garcia 1998, 2001; Aschwanden and Alexander 2001; Battaglia et al. 2005; Sylwester et al. 1995; Veronig and Brown 2004; Veronig et al. 2005; Yamamoto and Sakurai 2010). In summary, SOC theory represents an important statistical tool to link physical modeling to observed correlations

(scaling laws) and size distributions.

4.4. Soft X-ray versus Hard X-ray Flare Statistics

A compilation of hard X-ray flare statistics over the last three solar cycles has been conducted in a recent study (Aschwanden 2011b and references therein). The following powerlaw slopes have been found for the hard X-ray parameters: $\alpha_P = 1.73 \pm 0.07$ for the hard X-ray peak flux P , $\alpha_E = 1.62 \pm 0.12$ for the total time-integrated hard X-ray flux (or fluence) E , $\alpha_T = 1.99 \pm 0.35$ for the hard X-ray flare durations T . These results agree remarkably well with our FD-SOC model, which predicts $\alpha_P = 5/3 \approx 1.67$, $\alpha_E = 3/2 = 1.50$, and $\alpha_T = 2.00$ for the 3D case (Aschwanden 2012; Table 1 therein). Comparing hard X-ray with soft X-ray flare statistics, we have to be aware that the peak fluxes in these two wavelengths are not equivalent. The peak of the hard X-ray flux light curve $f_{hxr}(t)$ represents a maximum fluctuation of the instantaneous energy dissipation rate (if the temporal fluctuations are fully resolved in time), while the peak flux in soft X-rays represents the maximum value of the smoothed energy dissipation rate, because the intermittent and spiky instantaneous energy dissipation rate is convolved with a cooling time, which has a smoothing effect on the light curve, as demonstrated in Fig. 7. Therefore, our FD-SOC model predicts a steeper slope $\alpha_F = 2.0$ for the soft X-ray peak flux distribution than the slope $\alpha_P = 1.67$ for the hard X-ray peak flux distribution, which is indeed confirmed with the observed data.

In an earlier study (Lee et al. 1995) it was suspected that the size distribution of the soft peak flux (with powerlaw slope α_F) should correspond to the size distribution of the (time-integrated) hard X-ray fluence α_E , according to the Neupert effect, which predicts

$$f_{sxr}(t) = \int_0^t f_{hxr}(t') dt' , \quad (21)$$

but the data were found to contract this expectation (Lee et al. 1995). This failure corroborates that the integral formulation (Eq. 21) of the Neupert effect is an oversimplified approximation and does not hold on a statistical basis. A more accurate approximation is the formulation of the Neupert effect in terms of a convolution of the hard X-ray flux with a finite e-folding cooling time, as expressed with Eq. (11). Such a relationship is consistent with the predictions of our FD-SOC model, which predicts a powerlaw slope of $\alpha_F = 2.0$ for the soft X-ray peak flux and a powerlaw slope of $\alpha_E = 1.5$ for the hard X-ray fluence (while the Neupert effect would predict both to have an identical value). The relationship between soft X-ray and hard X-ray fluxes has also been quantified in some statistical studies (e.g., Battaglia and Benz 2006; McTiernan 2009; Falewicz et al. 2009).

The powerlaw slope α_P of the hard X-ray peak flux was found to vary slightly with the solar cycle, between a minimum value of $\alpha_P = 1.62 \pm 0.02$ in the decay phase of a solar cycle to $\alpha_P = 1.79 \pm 0.02$ during the minimum or rise of the solar cycle (Aschwanden 2012a). However, this variation is about of the same order as the differences between the three different instruments (SMM, CGRO, RHESSI) and three different flare detection methods used for the statistics. Since we find that some soft X-ray parameters are invariant during the solar cycle, while other parameters vary due to the flare pile-up bias, it is not clear at this point whether the variation of hard X-ray powerlaws is also caused by the flare pile-up bias, or if it is related to intrinsic variations of the self-organized criticality conditions (Aschwanden 2011c).

4.5. Solar Flare Predictability

The occurrence frequency distributions we obtained from the GOES soft X-ray fluxes are also called probability distribution functions (PDF) and can be used for statistical flare prediction. The fact that we established here the invariance of the powerlaw slope, makes the statistical prediction very easy, because the number of flares observed or to be predicted depends only on one single time-dependent parameter, the scaling factor N_1 ,

$$N(P)dP = N_1(t) \left(\frac{P}{P_1} \right)^{-\alpha_P} dP = N_1(t) \left(\frac{P}{P_1} \right)^{-2} dP, \quad (22)$$

where P_1 is an absolute constant, say $P_1 = 10^{-6} \text{ Wm}^{-2}$ for the C-class level, and $N_1(t)$ is the number of flares observed at this level in the interval dP . Forecasting the number of flares that are larger than a given threshold level, are given by the cumulative PDF,

$$N^{cum}(> P) = \int_P^\infty N_1(t) \left(\frac{P}{P_1} \right)^{-2} dP = N_1(t) \left(\frac{P}{P_1} \right)^{-1}. \quad (23)$$

The time-varying function $N_1(t)$ can be measured at any level P_1 within the powerlaw range. This time-varying function $N_1(t)$ can be broken down for different active regions and be turned on and off individually for each active region in a prediction model, depending on their appearance on the east-side of the Sun or disappearance on the west-side. Thus, the accuracy of forecasting depends only on the temporal extrapolation of the flaring rate $N_1(t)$ per active region, which can also be trended from statistical variations.

Predicting the largest event in history or future is a delicate issue. In principle we can take the mean of the largest events during each solar cycle as a reasonable guess for the next solar cycle, which yields something like an X20 GOES class. The solar dynamo resets the magnetic field after every 11-year cycle, so that no nonpotential magnetic field can be stored on longer terms, potentially leading to larger giant flares. What the SOC theory tells us in addition is the scaling of the flare energy with the length scale, which simply scales with the fractal volume, $E \propto V_S \propto L^{D_S}$. Once the size scale L is measured for the largest flares, we can scale the maximum possible flare energy by the maximum scale size L_{max} , which probably corresponds to the maximum active region size L_{AR} . Active regions grow and wane in size, $L_{AR}(t)$, which can be used to estimate the maximum flare rate $N_1(t)$ per active region, and this way be used in the prediction of the cumulative PDF of flares above some size (Eq. 23).

5. CONCLUSIONS

In order to obtain a deeper physical understanding of nonlinear dissipative systems governed by self-organized criticality (SOC) we need large statistics of SOC parameters to accurately quantify their statistical probability distribution functions (PSF) and the scaling laws between SOC parameters. For this purpose we analyzed the largest available, uniformly sampled dataset of solar flare light curves from the GOES spacecraft series over the last 37 years (1974-2012). Analyzing this dataset and applying the fractal-diffusive self-organized criticality model (FD-SOC) we arrived at the following major conclusions:

1. With an automated flare detection algorithm applied to the GOES 1-8 Å light curves we detect a total of 338,661 flare events during the epoch of 1975-2011 that includes all full years with GOES records. Our algorithm detects about 5 times more solar flares (with a noise level at the GOES A2-class level) than the official GOES flare catalog issued by NOAA, which covers the epoch of 1991-2012. The duty cycle of GOES is found to be $94\% \pm 4\%$ during the years 1978-2011.

2. The occurrence frequency distributions of GOES flare parameters can be characterized by a powerlaw function with a gradual turnover at the lower end, which can be characterized and fitted with the function $N(x) = N_1(1 + x/x_1)^{-\alpha}$, in order to obtain an accurate powerlaw slope corrected for the turnover. We find the following mean powerlaw slopes: $\alpha_F = 1.98 \pm 0.11$ for the soft X-ray peak flux F , $\alpha_T = 2.97 \pm 0.71$ for the soft X-ray rise time T , and $\alpha_{df/dt} = 2.01 \pm 0.12$ for the steepest time derivative during the soft X-ray rise time.
3. The powerlaw slopes of the (background-subtracted) peak flux F and of the time derivative (df/dt) are found to be invariant during the last three solar cycles with a variation of less than 5%. The powerlaw slope of the soft X-ray rise time T and the turnover values ($F_1, df/dt_1, T_1$) are all found to vary systematically with the solar cycle and can be modeled with the flare pile-up bias effect, which causes a loss of small flares and an underestimate of the flare duration (defined by the rise time here) during times of high flare rates. The flare rate of years during the solar minimum, however, are not affected by the flare pile-up bias, during which we measure a powerlaw slope of $\alpha_T = 2.02 \pm 0.04$ for the soft X-ray rise time T .
4. The fractal-diffusive self-organized criticality (FD-SOC) model (Aschwanden 2011a) predicts a fractal dimension of $D_3 = 2.0$ for flare volumes and powerlaw distributions with slopes of $\alpha_F = 2.0$ for the (smoothed) peak flux F and $\alpha_T = 2.0$ for the flare duration, which are both consistent with the observations (taking the flare pile-up effect into account). Most previous studies are also consistent with our results and the FD-SOC model (if we take flare pile-up effects into account), except those with small-number statistics or no background subtraction.
5. The consistency of the observations with the theoretical (FD-SOC) model implies also a powerlaw distribution for the time-integrated dissipated flare energy with a powerlaw slope of $\alpha_E = 1.5$, which rules out that nanoflares contribute significantly to coronal heating (which would require a powerlaw slope of $\alpha_E > \alpha_{crit} = 2.0$.)
6. The theoretical FD-SOC model predicts the powerlaw distributions of the instantaneous energy dissipation rate F , the peak dissipation rate P , the time-integrated energy release volume E , the time duration T , the fractal dimension D_S of the avalanches volume V_S , and scaling laws between these spatial and temporal parameters of SOC avalanches. The prediction of the size distributions of observables, such as the soft X-ray flux F_{sxr} or hard X-ray flux F_{hxr} requires a physical model of the emissivity per volume element, which entails thermal and non-thermal emission. For soft X-ray data we find that the soft X-ray intensity F_{SXR} is proportional to the instantaneous energy dissipation rate F , which implies a balance between the plasma heating rate and the radiative loss rate.
7. The hard X-ray peak fluxes have a powerlaw slope $\alpha_P \approx 1.7$ that is different from the powerlaw slope $\alpha_F = 2.0$ of the soft X-ray peak flux, but both values are consistent with the FD-SOC theory. The difference can be understood by the fact that the hard X-ray peak flux represents the most extreme fluctuation of the energy dissipation rate during a flare, while the soft X-ray peak flux represents a convolution function with an e-folding cooling time, which smoothes out the fluctuations of the intermittent energy dissipation rate. The integral formulation of the Neupert effect appears to be an oversimplification that is not consistent with the data, but a formulation in terms of a convolution of the hard X-ray flux with an e-folding cooling time seems to be more realistic and is consistent with the FD-SOC model.
8. The invariance of the soft X-ray peak flux powerlaw slope ($\alpha_F = 2$) during the solar cycles simplifies the statistical prediction of solar flares, since the statistical expectation value is then proportional for

every flux level. The cumulative occurrence frequency distribution has a slope of $\beta_F = \alpha_F - 1 = 1$, which states that the probability of a flare greater than a flux level F drops reciprocally with the flux level F . An X-class flare is 100 times less likely than a C-class flare. The largest flares in history or future are unlikely to surpass the largest flares observed hitherto, based on the fact that the FD-SOC model predicts a dependence of the released energy on the flare size, which is limited by the largest system size, i.e., the largest active region in the case of solar flares.

If the reader goes back to the eight questions at the beginning of the Introduction, he/she will find that we arrived at a quantitative answer to almost all questions. Nevertheless, there are more open questions: How can we understand the solar cycle variation of the hard X-ray powerlaw slope? What is the physical scaling between the (fractal) avalanche volume and the emissivity in different wavelengths (soft X-rays, hard X-rays, gamma-rays, EUV)? How do the scaling laws between different forms of flare energies relate to each other (thermal, non-thermal, kinetic, magnetic energy)? Does a more extended flare energy distribution spanning over 8 orders of magnitude from the largest flare to the smallest detectable nanoflares exhibit a single powerlaw slope? Can we statistically verify the fractal spatial geometry and scaling laws with imaging observations of solar flares? Future studies with multi-wavelength data from AIA/SDO are expected to shed more light on these problems.

The first author acknowledges helpful discussions with Karel Schrijver and Greg Slater. We thank the data services at NOAA, NASA/GSFC Solar Data Analysis Center (SDAC), SSW support, and the individuals who contributed to the GOES/SSW database, in particular Joe Gurman, Kim Tolbert, Dominic Zarro, Richard Schwartz, and Mons Morrison.

REFERENCES

- Aschwanden, M.J. 1994, *Solar Phys.* 152, 53.
- Aschwanden, M.J. and Alexander, D. 2001, *Solar Phys.* 204, 91.
- Aschwanden, M.J. 2004, *Physics of the Solar Corona. An Introduction*, PRAXIS Publishing Co., Chichester UK, and Springer, Berlin.
- Aschwanden, M.J. 2011a, *Self-Organized Criticality in Astrophysics. The Statistics of Nonlinear Processes in the Universe*, Praxis-Springer, Berlin, ISBN 978-3-642-15000-5, 416p.
- Aschwanden, M.J. 2011b, *Solar Phys.* 274, 99.
- Aschwanden, M.J. 2011c, *Solar Phys.* 274, 119.
- Aschwanden, M.J. 2012, *A&A* 539, A2, 15p.
- Bak, P., Tang, C., and Wiesenfeld, K. 1987, *PhRvL* 59/4, 381.
- Bak, P., Tang, C., and Wiesenfeld, K. 1988, *PhRvA* 38/1, 364.
- Bak, P. 1996, *How Nature Works*, Copernicus, Springer-Verlag, New York.
- Battaglia, M., Grigis, P.C., and Benz, A.O. 2005, *A&A* 439, 737.
- Battaglia, M. and Benz, A.O. 2006, *A&A* 456, 751.
- Benz, A.O. 1985, *SP* 96, 357.
- Bornmann, P.L. 1990, *ApJ* 356, 733.

- Bouwer,S.D., Donnelly,R.F., Falcon,J., Quintana,A., and Caldwell,G. 1982, NOAA TM, ERL SEL-62.
- Charbonneau, P., McIntosh, S.W., Liu, H.L., and Bogdan, T.J. 2001, Solar Phys. 203, 321.
- Crosby, N.B., Aschwanden, M.J. and Dennis, B.R. 1993, Solar Phys. 143, 275.
- Crosby, N.B. 2011, Nonlinear Processes in Geophysics 18/6, 791.
- Dennis, B.R. and Zarro, D.M. 1993, Solar Phys. 146, 177.
- Dennis, B.R., Veronig, A., Schwartz, R.A., Sui, L., Tolbert, A.K., Zarro,D.M. and the RHESSI Team 2003, Adv.Space Res. 32, 2459.
- Donnelly, R.F., Grubb, R.N., and Cowley, F.C. 1977, NOAA TM ERL/SEL-48.
- Drake,J.F. 1971, Solar Phys. 16, 152.
- Drake, J.F., Swisdak, M., Che,H., Shay, M.A. 2006a, Nature 443, 553.
- Drake, J.F., Swisdak, M., Schoeffler,B.N., Rogers, S., Kobayashi, S, 2006b, GRL 33, 13105.
- Falewicz,R., Rudawy,P., Siarkowski,M. 2009, A&A 500, 901.
- Feldman, U., Doschek, G.A., and Klimchuk, J.A. 1997, ApJ 474, 511.
- Freeland, S.L. and Handy, B.N. 1998, Sol. Phys.182, 497.
- Garcia, H.A. 1994, Solar Phys. 154, 275.
- Garcia, H.A. 1998, ApJ 504, 1051.
- Garcia, H.A. 2001, ApJ 557, 897.
- Grubb, R.N. 1975, NOAA TM ERL SEL-42.
- Hergarten, S. 2002, *Self-Organized Criticality in Earth Systems*, Springer, Berlin.
- Hill, S.M. and 35 co-authors 2005, Solar Phys. 226, 255.
- Hudson, H.S., Peterson, L.E., and Schwartz, D.A. 1969, ApJ 157, 389.
- Hudson, H.S. 1991, Solar Phys. 133, 357.
- Jensen, H.J. 1998, *Self-Organized Criticality: Emergent complex behaviour in physical and biological systems*, Cambridge University Press.
- Kahler,S.W. and Kreplin,R.W. 1991, Solar Phys. 133, 371.
- Karpen, J.T., Antiochos, S,K., and DeVore, C.R. 1995, ApJ 450, 422.
- Kliem, B. 1990, Astron.Nachr. 311/6, 399.
- Leboef, J.N., Tajima, T., Dawson, J.M. 1982, PhFl 25, 784.
- Lee, T.T., Petrosian, V., and McTiernan, J.M. 1995, ApJ 418, 915.
- Lu, E.T. and Hamilton, R.J. 1991, ApJ 380, L89.
- McTiernan, J.M. 2009, ApJ 697, 94.
- Metcalf, T.R., and Fisher, G.H. 1995, ApJ 462, 977.
- Neupert, W.M. 2011, Solar Phys. 272, 319.
- Phillips,K.J.H., and Feldman,U. 1995, A&A 304, 563.
- Pizzo, V.J., Hill, S. M., Balch, C. C., Biesecker, D. A., Bornmann, P., Hildner, E., Grubb, R. N., Chipman, E. G., Davis, J. M., Wallace, K. S., Russell, K., Cauffman, S. A., Saha, T. T., and Berthume, G. D. 2005, Solar Phys. 226, 283.

- Pruessner, G. 2012, *Self-organised criticality*, Cambridge University Press, Cambridge, UK.
- Shibata, K. and Tanuma, S. 2001, EPS 53, 473.
- Shimizu, T. 1995, PASJ 47, 251.
- Shimojo, M. and Shibata, K. 1999, ApJ 516, 934.
- Shing, L., Stern, R.A., Catura, P., Morrison, M.D., Eaton, T. and Pool, P.J. 1999, SPIE 3765, 299.
- Sornette, D. 2004, *Critical phenomena in natural sciences: chaos, fractals, self-organization and disorder: concepts and tools*, Springer, Heidelberg, 528 p.
- Sturrock, P.A. 1966, Nature 5050, 695.
- Sylwester, J., Garcia, H.A., and Sylwester, B. 1995, A&A 293, 577.
- Tajima, T., Sakai, J., Nakajima, H., Kosugi, T., Brunel, F., and Kundu, M.R. 1987, ApJ 321, 1031.
- Thomas, R.J., Starr, R., and Crannell, C.J. 1985, Solar Phys. 95, 323.
- Turcotte, D.L. 1999, *Self-organized criticality*, Rep. Prog. Phys. 62, 1377.
- Veronig, A.M., Temmer, M., Hanslmeier, A., Otruba, W., and Messerotti, M. 2002a, A&A 382, 1070.
- Veronig, A.M., Temmer, M., and Hanslmeier, A. 2002b, Hvar Observatory Bulletin, 26, 7.
- Veronig, A.M., Temmer, M., and Hanslmeier, A. 2004, Solar Phys. 219, 125.
- Veronig, A.M. and Brown, J.C. 2004, ApJ 603, L117.
- Veronig, A.M., Brown, J.C., Dennis, B.R., Schwartz, R.A., Sui, L., and Tolbert, A.K. 2005, ApJ 621, 482.
- Wagner, W.J. 1988, Adv. Space Res. 8/7, 67.
- White, S.M., Thomas, R.J., and Schwartz, R.A. 2005, Solar Phys. 227, 231.
- Wolfram S. 2002, *A New Kind of Science*, Wolfram Media, ISBN 1-57955-008-8.
- Yamamoto, T.T., and Sakurai, T. 2010, PASJ 62, 755.
- Yashiro, S., Akiyama, S., Gopalswamy, N., and Howard, R. A. 2006, ApJ 650, L143.

Table 1. Powerlaw slopes of occurrence frequency distributions detected with GOES per year.

Year	Number of events	Number of NOAA events	Duty cycle	Powerlaw slope peak flux α_F	Powerlaw slope rise time α_T	Powerlaw slope derivative $\alpha_{df/dt}$
Mean	9153	1804	0.922	1.98±0.11	2.97±0.71	2.01±0.12
1975	2865	0.794	2.04±0.10	2.24±0.04	1.98±0.08
1976	1827	0.670	1.82±0.07	2.13±0.02	1.89±0.06
1977	5543	0.818	1.91±0.04	2.43±0.06	1.96±0.05
1978	16897	0.923	1.92±0.01	2.76±0.07	1.95±0.04
1979	18797	0.910	2.00±0.03	3.18±0.10	2.04±0.04
1980	15340	0.843	2.10±0.04	2.72±0.05	2.13±0.03
1981	15527	0.871	2.07±0.02	3.22±0.09	2.05±0.01
1982	15963	0.914	1.96±0.04	2.89±0.03	1.96±0.02
1983	9566	0.897	2.04±0.03	2.72±0.03	2.01±0.03
1984	6894	0.873	1.95±0.01	2.77±0.03	1.99±0.05
1985	2776	0.904	1.98±0.07	2.37±0.05	1.87±0.06
1986	2337	0.900	1.87±0.04	2.27±0.01	2.03±0.09
1987	4863	0.865	2.11±0.07	2.67±0.05	1.98±0.06
1988	13030	0.947	2.07±0.03	3.24±0.11	2.10±0.03
1989	17535	0.938	2.00±0.04	3.81±0.10	2.03±0.04
1990	15280	0.944	2.13±0.02	3.44±0.55	2.11±0.03
1991	16860	2124	0.943	2.02±0.03	3.29±0.08	2.02±0.01
1992	12488	4434	0.933	1.96±0.04	3.17±0.09	2.01±0.02
1993	9386	3181	0.902	2.02±0.02	3.41±0.21	2.11±0.05
1994	4844	1694	0.958	2.03±0.03	2.64±0.03	2.10±0.02
1995	2650	1067	0.847	1.99±0.02	2.58±0.05	1.96±0.05
1996	1288	551	0.937	1.93±0.06	2.20±0.03	2.00±0.05
1997	3776	1148	0.973	1.99±0.04	2.51±0.05	1.98±0.06
1998	11172	2256	0.978	1.96±0.04	3.26±0.12	2.04±0.02
1999	14685	2377	0.976	2.12±0.04	3.02±0.13	2.17±0.05
2000	16156	2661	0.972	2.04±0.03	4.61±0.15	2.10±0.03
2001	16022	2710	0.979	1.97±0.02	3.51±0.62	2.03±0.06
2002	16167	2670	0.965	2.07±0.05	5.18±0.55	2.15±0.04
2003	12283	2395	0.978	1.85±0.02	3.82±0.19	1.85±0.03
2004	8956	2368	0.962	1.88±0.04	3.12±0.11	1.95±0.03
2005	6706	2029	0.970	1.77±0.01	3.19±0.16	1.83±0.02
2006	3100	1200	0.983	1.89±0.06	2.43±0.03	1.92±0.04
2007	1434	651	0.947	1.88±0.05	2.17±0.02	2.00±0.05
2008	186	88	0.981	1.69±0.07	1.75±0.05	1.72±0.04
2009	528	245	0.979	2.31±0.14	1.99±0.05	2.48±0.06

Table 1—Continued

Year	Number of events	Number of NOAA events	Duty cycle	Powerlaw slope peak flux α_F	Powerlaw slope rise time α_T	Powerlaw slope derivative $\alpha_{df/dt}$
2010	3662	1261	0.965	1.92 ± 0.06	3.76 ± 0.69	1.91 ± 0.06
2011	11272	2171	0.973	2.00 ± 0.03	3.29 ± 0.41	2.02 ± 0.03

Table 2. Frequency distributions measured from solar flares in soft X-rays. References: ¹⁾ Hudson et al. (1969); ²⁾ Drake et al. (1971); ³⁾ Shimizu (1995); ⁴⁾ Lee et al. (1995); ⁵⁾ Feldman et al. (1997); ⁶⁾ Shimojo and Shibata (1999); ⁷⁾ Veronig et al. (2002b); ⁸⁾ Veronig et al. (2002a); ⁹⁾ Yashiro et al. (2006); ¹⁰⁾ This work; ¹¹⁾ Aschwanden (2012); Data analysis with no background subtraction are marked with the symbol *.

Powerlaw slope of peak flux α_P	Powerlaw slope of total fluence α_E	Powerlaw slope of durations α_T	log size range	Number of events	Instrument	Reference
≈ 1.85			1	≈ 177	OSO-3	1)
1.84 (1.66)	1.44		2	3,140	Explorer	2)
1.80 (1.68)	1.5-1.6		2	291	Yohkoh	3)
1.79			2	?	SMM/BCS	4)
1.86			2	4,356	GOES	4)
1.88 ± 0.21			3	1,054	GOES	5)
1.7 ± 0.4			2	92	Yohkoh	6)
1.98 ± 0.08	1.89 ± 0.10		3	?	GOES	7,8)
$2.11 \pm 0.13^*$	$2.03 \pm 0.09^*$	$2.93 \pm 0.12^*$	3	49,409	GOES	8)
$2.16 \pm 0.03^*$	$2.01 \pm 0.03^*$	$2.87 \pm 0.09^*$	3	5,890	GOES	9)
1.98 ± 0.11		2.01 ± 0.12	4	327,389	GOES	10)
2.0	1.5	2.0		-	Theory	11)

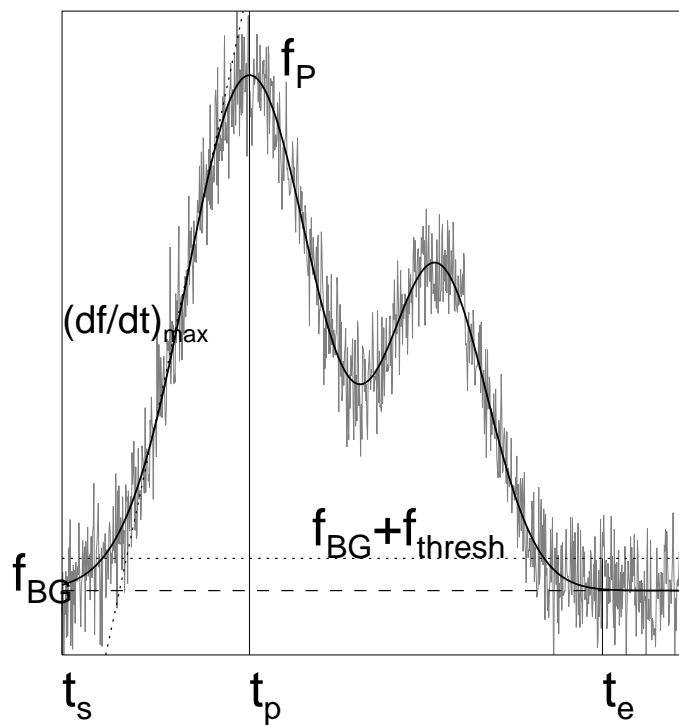


Fig. 1.— Schematic of flare parameters: flare start time t_s , flare peak time t_p , flare end time t_e , preflare background f_{BG} , flux threshold f_{thresh} , flare peak flux f_P , and maximum flux-time derivative $(df/dt)_{max}$. The curve with thick linestyle represents the rebinned and smoothed light curve which defines the local flux maxima and minima.

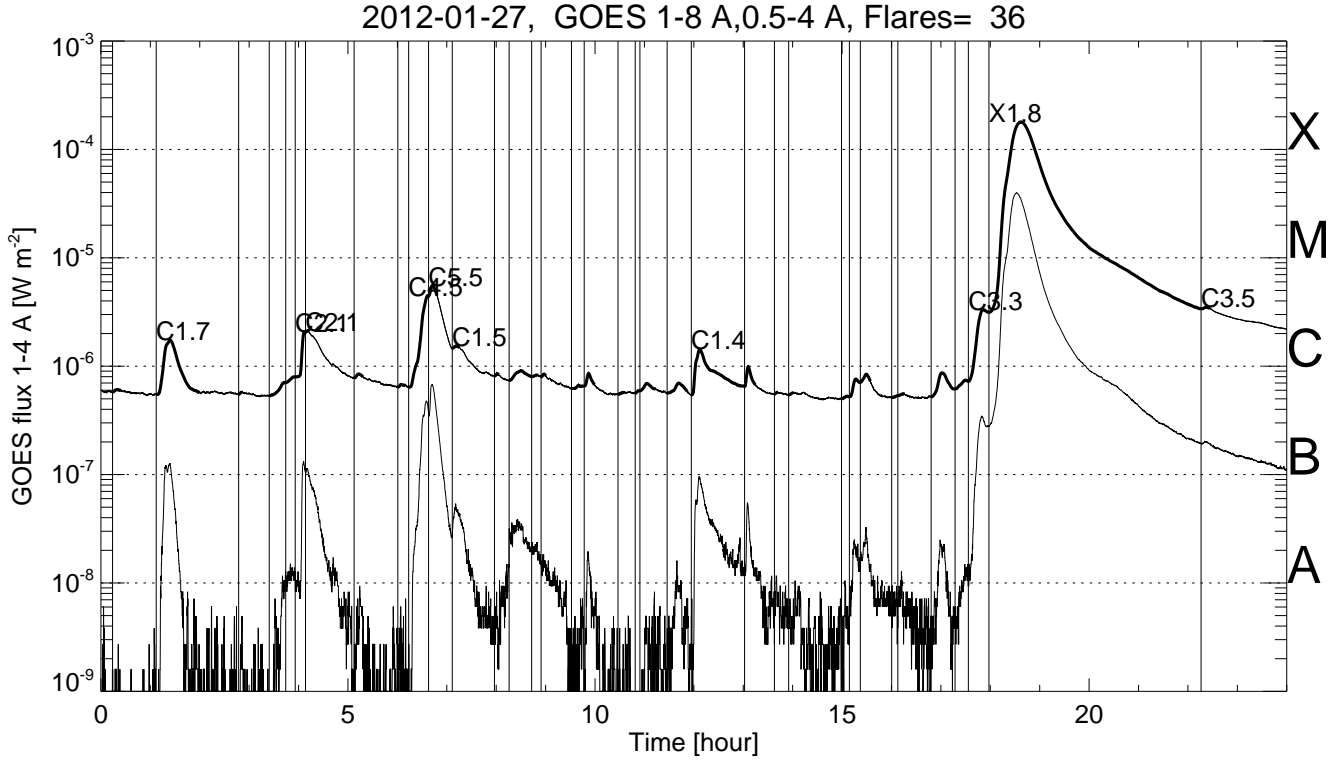


Fig. 2.— Example of automated flare detection of GOES observations during the day of 2012-Jan-27, which featured an X1.8 flare. A number of 36 flares are detected down to the GOES B5-class level (with the starting times t_s marked with vertical bars). Only flares with a GOES class of $> C1.0$ are labeled. The upper light curve is the 1-4 Å wavelength range, which is used for flare detection, while the lower curve shows the 0.5-8 Å data.

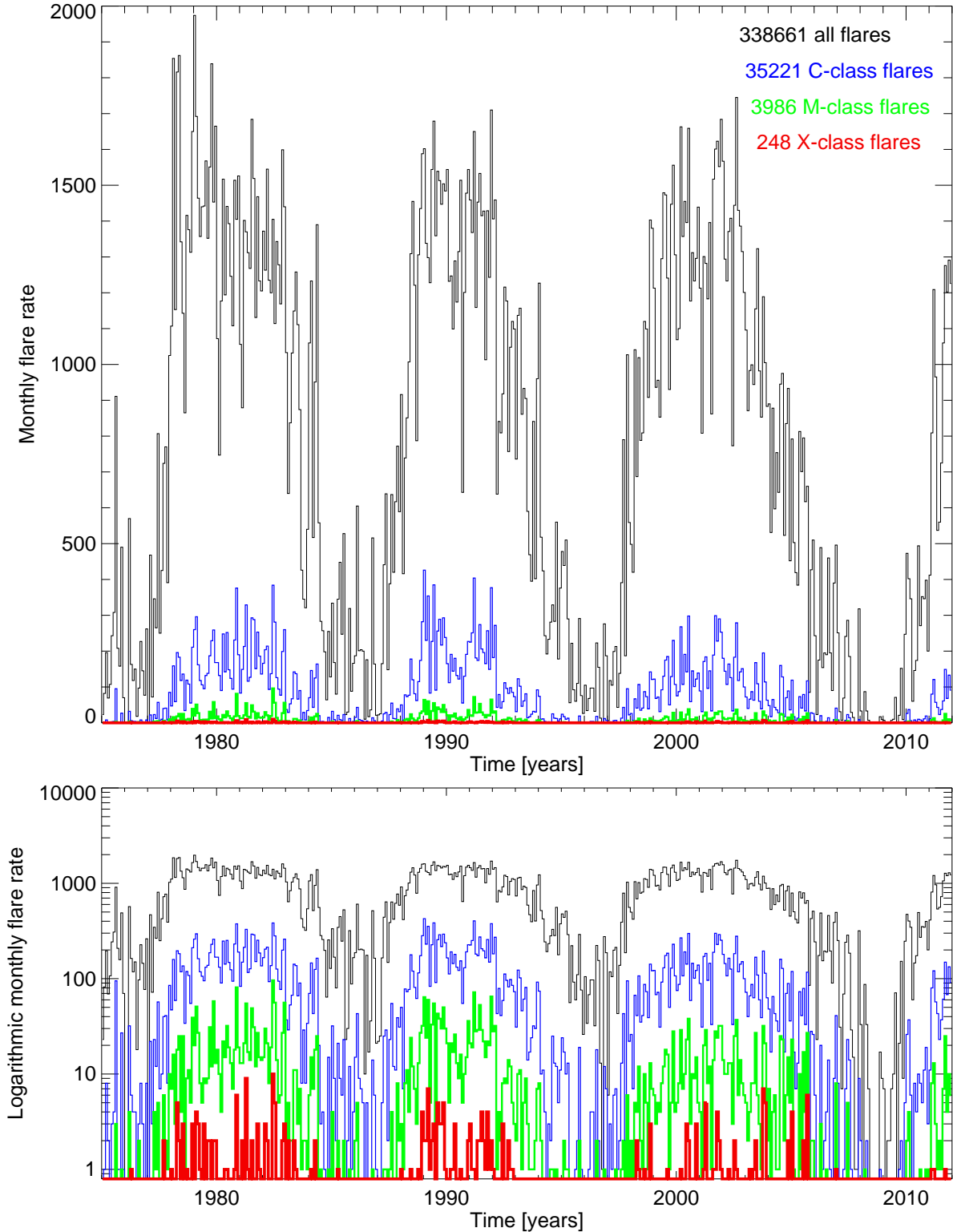


Fig. 3.— Monthly flare rate during 1975-2011 on a linear scale (top panel) and on a logarithmic scale (bottom panel). The rate of C (blue), M (green), and X-class flares (red) are shown in colors. Note the proportionality of detected flares in different magnitudes.

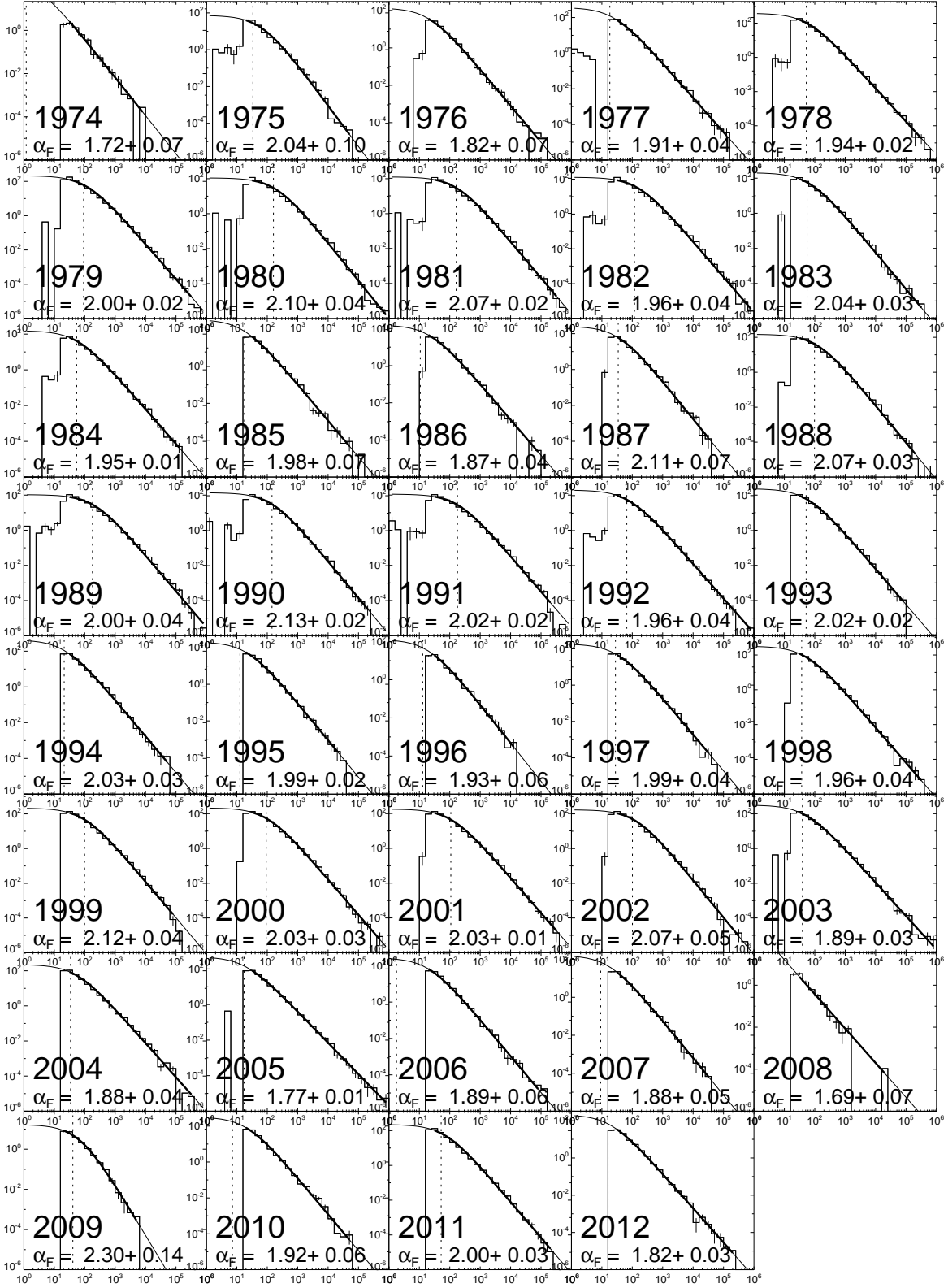


Fig. 4.— Occurrence frequency distributions of GOES 1-4 Å peak fluxes of solar flares detected by year. The powerlaw slope α_F is indicated for each year. Incomplete years are the first (1974 Nov-Dec) and the last one (2012 Jan-Mar).

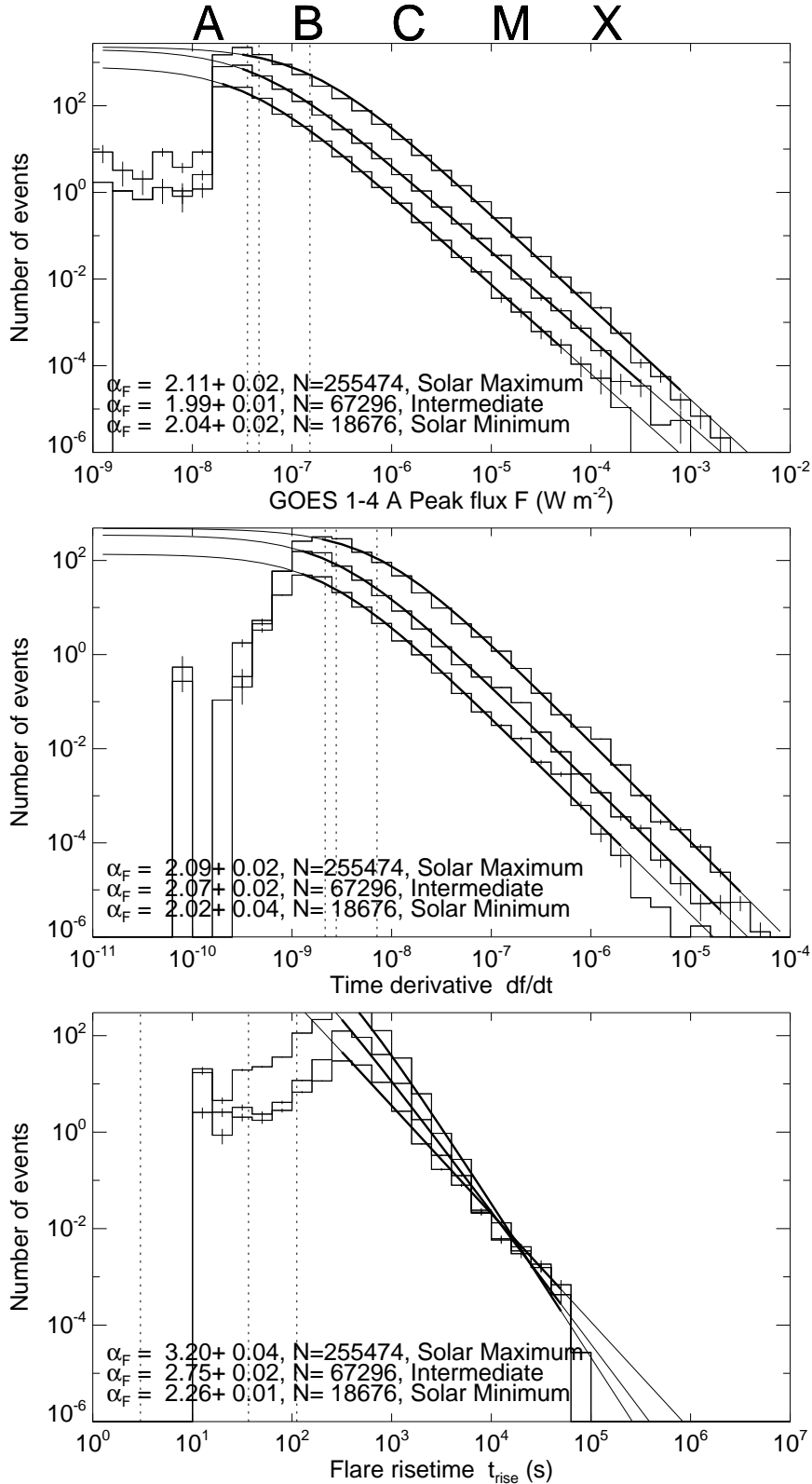


Fig. 5.— Occurrence frequency distribution of the GOES 1-4 Å peak fluxes (top panel), the time derivative $(df/dt)_{max}$ (middle panel), and flare rise times t_{rise} during the solar cycle maximum (years with $N_{ev} \geq 10000$ events), the solar cycle minimum (years with $N_{ev} < 3000$ events), and for intermediate years. Note the invariance of the powerlaw slope for the peak fluxes (top panel) and time derivatives (middle panel).

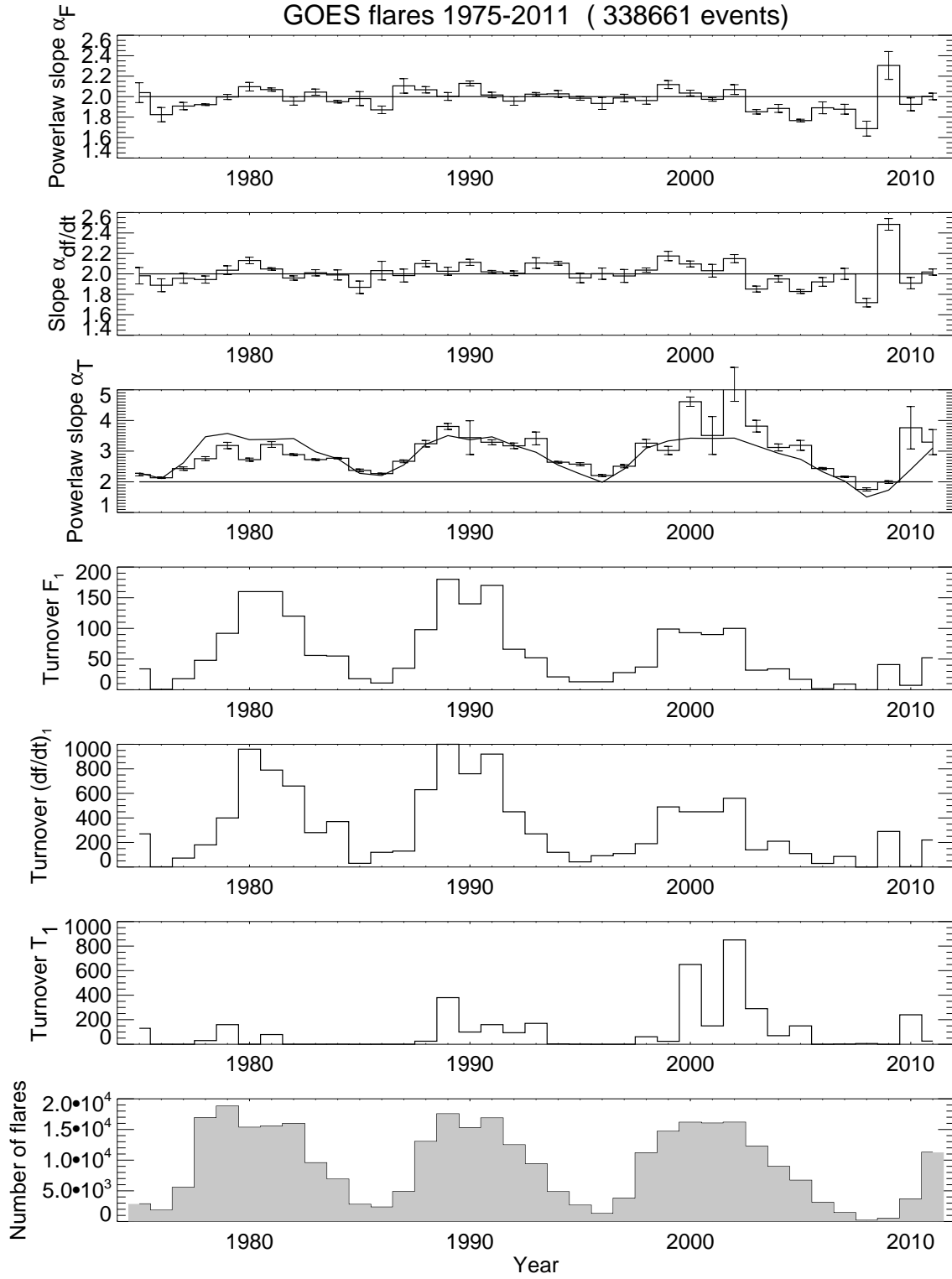


Fig. 6.— Variation of powerlaw slopes $\alpha_F(t)$, flux-time derivative $\alpha_{df/dt}(t)$, rise time $\alpha_T(t)$, turnover flux value F_1 (in units of 10^{-9} W m^{-2}), turnover value of time derivative $(df/dt)_1$, (in units of $3 \cdot 10^{-11} \text{ W m}^{-2} \text{ s}^{-1}$), turnover value of rise time $T_1(t)$ (in units of s), and flare rate $N_{flare}(t)$ during the three last solar cycles. The theoretically predicted values are marked with thick solid lines.

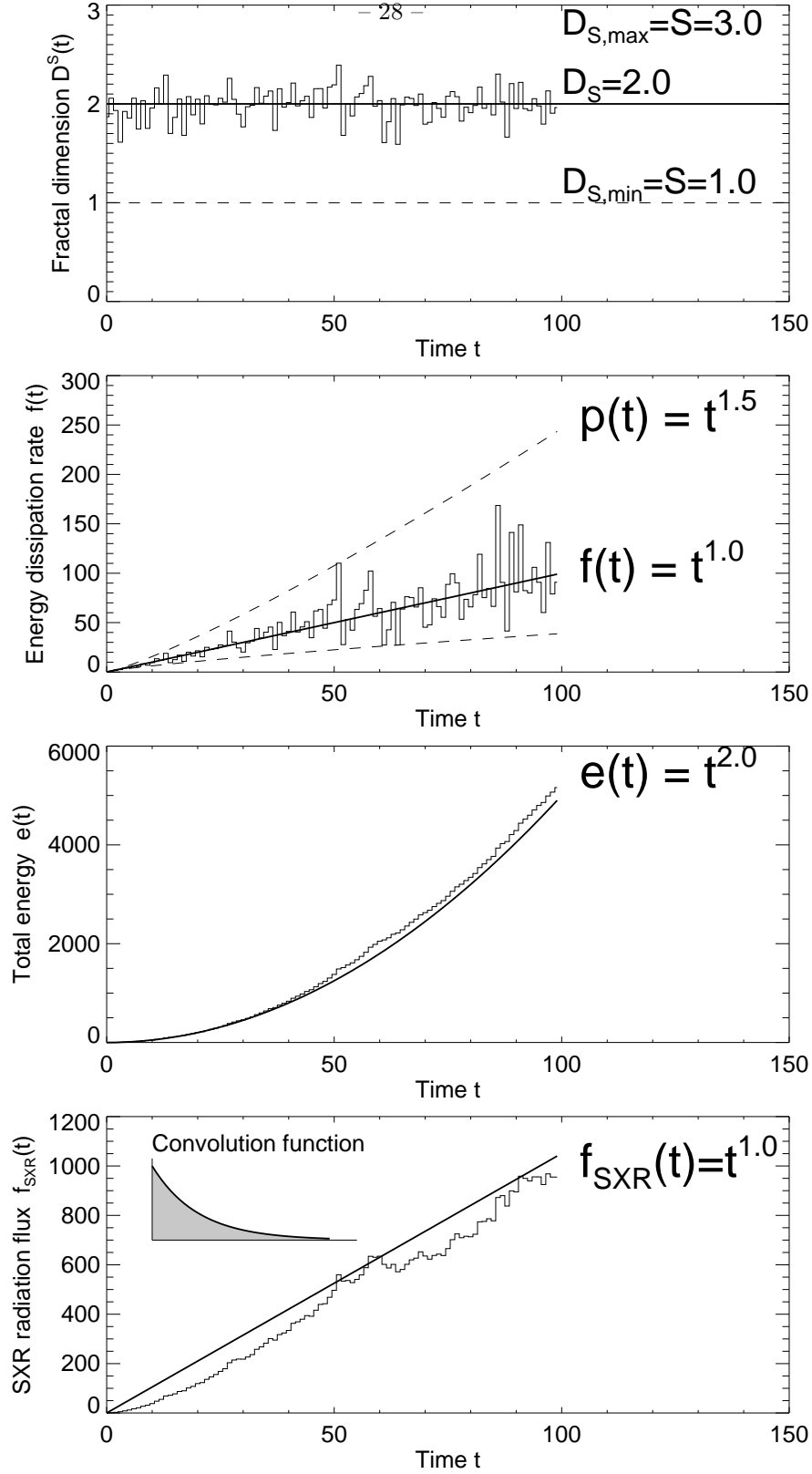


Fig. 7.— Simulation of the fractal-diffusive SOC model for an Euclidean dimension $S = 3$, showing the time evolution of the fractal dimension $D_S(t)$ (top panel), the instantaneous energy dissipation rate $f(t)$ and peak energy dissipation rate $p(t)$ (second panel), the total time-integrated dissipated energy $e(t)$ (third panel), and the soft X-ray time profile $f_{\text{SXR}}(t)$ (bottom panel), which results from the convolution of the instantaneous energy dissipation rate $f(t)$ (second panel) with an exponential decay function with an e-folding time of $\tau_{\text{decay}} = 20$ (shown in insert of bottom panel).